Circuits, Systems, and Signal Processing (2023) 42:5453–5477
https://doi.org/10.1007/s00034-023-02364-9

Orthogonal Signal Generation: An Analytical Approach

Jean-Marc Girault[1,2] · **Roberto Longo**[1,2] · **Sébastien Ménigot**[1,2]

Received: 13 June 2022 / Revised: 20 March 2023 / Accepted: 21 March 2023 /
Published online: 18 April 2023

Abstract
Nowadays, many signal processing activities are related to the orthogonal properties of specific signals. However, only a few methods offer an analytical solution for generating orthogonal signals, especially when only one input to the generating system is available. These methods are often related to very specific applications and lack generalization. In this paper, the use of the Gram–Schmidt orthogonalization process combined with simple transformation operators is proposed as a new framework for generating orthogonal signals. The objective is to provide a rigorous, clear and simple procedure capable of deriving multiple orthogonal signals from a single input. Many examples are discussed to better illustrate the novelty of the method and the main results.

Keywords Orthogonal Signal Generator · Orthogonalization · Analytical approach · Signal processing

1 Introduction

Today most high-performance signal processing approaches exploit orthogonality properties of signals in various contexts as in telecommunications [12, 17, 22], in system-control engineering [3, 5] and in electrical engineering [8, 11, 31], to make but a few. Orthogonality through the orthogonal functions is known to be the simplest

✉ Jean-Marc Girault
jean-marc.girault@eseo.fr

Roberto Longo
roberto.longo@eseo.fr

Sébastien Ménigot
sebastien.menigot@eseo.fr

1 Groupe Signal Image and Instrumentation (GSII), Groupe ESEO, 10 boulevard Jeanneteau, CS 90717, 40107 Angers CEDEX 2, France

2 Laboratoire d'Acoustique de l'Université du Mans (LAUM), UMR 6613, Institut d'Acoustique - Graduate School (IA-GS), CNRS, Le Mans Université, Le Mans, France

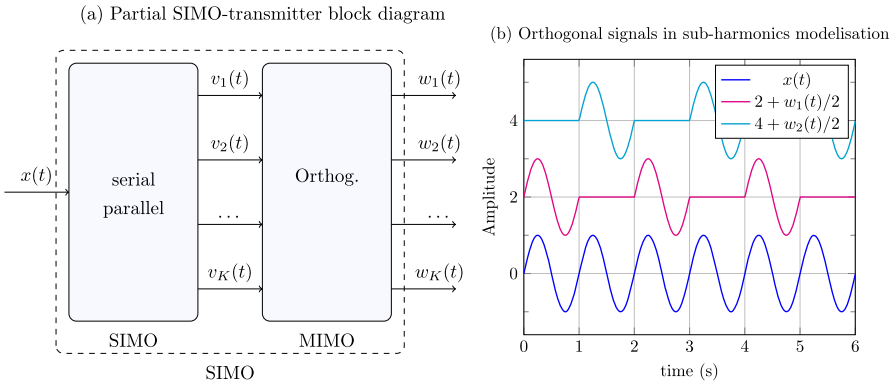

Fig. 1 **a** Partial block diagram of a transmission/modelization system as a single input multiple output (SIMO) system. This SIMO system can be separated in a serial-parallel converter (another SIMO system) followed by a MIMO (multiple input and multiple output) system composed of K mutually orthogonal signals. Usually, the orthogonalization function is merged with the serial/parallel function. **b** Orthogonal signals used in nonlinear systems modelization in control engineering with sub-harmonics [1, 25], with $x(t) = w_1(t) + w_2(t)$

way to ensure perfect discrimination between different signals. The method can be grouped into four families [6]: (i) piecewise constant orthogonal functions (Haar functions, Walsh functions,...), (ii) orthogonal polynomials (Legendre, Laguerre, Hermite, Tchebycheff, Jacobi, Gegenbauer,...), (iii) sine-cosine (Fourier) functions, (iv) various functions (Filtering,...).

In telecommunications, pre-existing orthogonal bases (usually calculated from orthogonal polynomials) composed of a large number of K channels [12, 17, 22] are used to account for several constraints simultaneously. The real-time constraint is the stronger, but other constraints are also important such as orthogonality in the complex domain, maximum spectral efficiency, and a well-localized prototype function in time and frequency. The common partial structure (see Fig. 1a) of a transmitter using orthogonalization can be represented by a single input and multiple out (SIMO) system with $x(t)$ at the input and $w_1(t)$, $w_2(t)$,..., $w_K(t)$ at the output. As reported in Fig. 1a, this SIMO system, constituting the basic structure of the solution of our problem, can be also separated in two sub-parts: (i) a serial-parallel converter (SIMO system) and (ii) a MIMO (multiple input and multiple output) system where orthogonalization takes place.

In control engineering, the SIMO structure plays an important role for the identification-modelling of linear systems [5, 6] and nonlinear systems [3] with sub-harmonics [1, 25], where pre-existing orthogonal functions are also used. In this case, the block diagram is similar to the one presented in Fig. 1a. To give an example, the orthogonal signals used in the modelling of subharmonics [1, 25] are presented in Fig. 1b.

In signal processing, the consideration of orthogonality has also been very fruitful. Many methods such as orthogonal matching pursuit [2, 21, 32], orthogonal least square [3] and orthogonal wavelet decomposition [19] have been developed, to name a few.

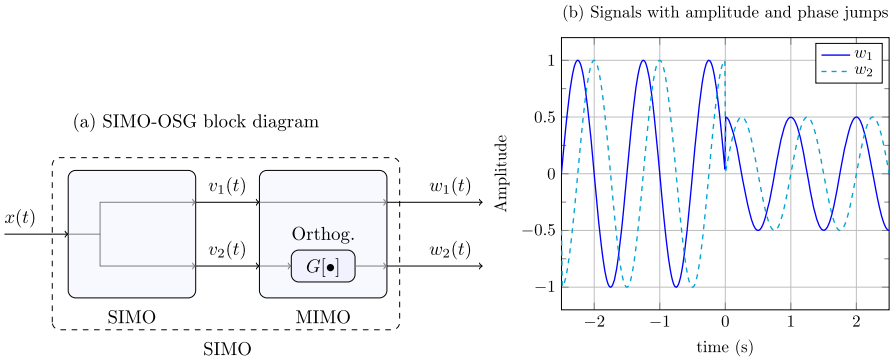

Fig. 2 **a** Common partial block diagram of a SIMO-OSG in electrical engineering. As in Fig. 1, the SIMO system can be separated in two sub-parts: another SIMO system followed by a MIMO system with $v_1(t) = w_1(t) = x(t)$, $v_2(t) = x(t)$ and with orthogonalized signal $w_2(t)$ being obtained through a transformation $G[\bullet]$ as derivative, Hilbert transform,... **b** Periodic signal $w_1 = x(t)$ undergoing a phase and an amplitude jumps at $t = 0$ and its orthogonalized version $w_2(t)$ obtained by applying the method of Sect. 2.1

More recently in electrical engineering [8, 11, 15, 16, 30, 31], accurately extracting the phase angle and frequency from the grid voltage is of vital importance to ensure stable operation of power electronic equipment connected to the grid. For phase detection, PLL-based systems are probably the most popular, especially those using an orthogonal signal generator (OSG). Here again, the SIMO structure has a special place in GSO-based systems. For instance, OSG under study is often composed of few outputs (usually $K = 2$) and a single input. The structure of a OSG is very similar to the one shown in Fig. 1a, except that $w_1(t) = v_1(t) = x(t)$. As an illustration, the OSG-SIMO system composed of two sub-parts (SIMO+MIMO) with two outputs and a single input is shown in Fig. 2a. For this type of application, the system must adapt itself in real time to various network disturbances such as voltage sags, phase and frequency jumps, and in the presence of harmonics. The other important point, even if it is not really explained, is that the output signals must present the same properties as the input signal. The periodic signal $x(t)$ at the input and the orthogonal version $w_2(t)$ at the output both undergo a phase jump (see Fig. 2b). Eventually, note that $w_1(t) = x(t)$ guarantees that the properties of $x(t)$ are preserved in $w_2(t)$.

Most of OSG (through the transformation $G[\bullet]$ in the block diagram of Fig. 2a) can be clustered into three categories of analytical methods. A table with several examples is reported in "Appendix A.7".

- **Filtering-based method** Different type of filters (or transformations $G[\bullet]$) can be considered, the all-pass filter [13], the Hilbert transform [10, 14, 23], the combination of a band-pass and low-pass filter [4]. With the objective of presenting only analytical calculations, the method based on Hilbert transform is presented alone. The Hilbert transform (see definition in "Appendix A.6")-based method takes advantage of the fact that any real signal $v_1(t)$, quadratically integrable, has a Hilbert transform $HT[v_1(t)]$ orthogonal to it: $v_1(t) \perp HT[v_1(t)]$; a demonstration being given in "Appendix A.4". In electrical engineering [23], the Hilbert transform can be used for periodic signals such sine signals (see Table 1 in "Appendix").

However, for a certain number of signals, the calculation of the Hilbert transform often leads to solutions with singularities that may prevent their practical use as is the case for rectangular signal (First raw in Table 1in "Appendix"). For other signals like exponential based signals (Gaussian function for instance), the Hilbert transform has no analytical solution and we resort to a numerical calculation (see Table (A.1), raw 7). As the successive use of the Hilbert transform[1] leads to a unique solution (with just a sign difference), this method cannot be used for K>2.

- **Derivative-based method** As the name indicates, the method applies only to differentiable signals with parity properties [28]. Indeed, if the signal under consideration is even/odd, the scalar product with its odd/odd derivative is null, as shown in "Appendix A.3". The idea of using the derivability properties of orthogonal signals [28] or orthogonal polynomials [20] is interesting and has received some attention in a discrete framework in telecommunications [12, 27] and in electrical engineering [7, 18], to name a few. For instance, the Gaussian signal (see definition in "Appendix A.6") is an even function, derivable with non-compact support.[2] It has a first derivative (see definition in "Appendix A.6") that is an odd function[3] whose integral over the entire real axis is null. Moreover, unlike to the method based on the Hilbert transform, there are as many solutions as the odd/even signal is derivable. However for certain signals, the number of distinct solutions can be limited to two as it is the case for the $\cos(\omega t)$ and $\sin(\omega t)$ signal. Note that for even/odd signals based on exponential (infinitely derivable function), there is an infinity of distinct solutions and orthogonal bases functions can be constituted as is the case of weighted Hermite polynomials (see definition in "Appendix A.6") used in the telecommunications field [12, 22]. In the case of discontinuous periodic signals such as a periodic square-wave or triangular signal, derivatives showing singularities limit their application. Alternative solutions are thus expected.
- **Block-pulse function method** A very simple way to guarantee the orthogonality between real signals of finite energy, with bounded support or not, consists in finding an adequate time shift [6, 33] guaranteeing the orthogonality between the generator signal and the created one. In the case of signals with bounded support, this can be guaranteed if the supports of its shifted versions are disjoint. This is the case, for example, by using a base of rectangular symbols (see Table 1 in "Appendix"). For instance, $\mathrm{Rect}_T(t)$ and $\mathrm{Rect}_T(t-T)$ are orthogonal since their respective support are disjoint leading to a null product and so to a null scalar product.

  If the signal does not present a compact support, one could implement a windowing operation in order to get a bounded support signal. Note that this operation can be performed in time or frequency domain. In telecommunications [22], to optimize the temporal or frequency band, the support can also be contiguous. Instead of per-

[1] $\tilde{v}_1(t) = HT[v_1(t)]$ and $HT[\tilde{v}_1(t)] = -v_1(t)$.

[2] Note that the support of a function is the part where the useful information is concentrated. The support is defined in the region where the function presents nonzero values. The Gaussian function does not have a compact support.

[3] The product of an even function $e(t) = e(-t)$ by an odd function $o(t) = -o(-t)$ leads to an odd function $y(t) = e(t) \times o(t) = -y(-t)$. Demonstration: $-y(-t) = -e(-t) \times o(-t) = -e(t) \times -o(t) = y(t)$, EQD.

forming a simple shift, we can also use more complex decomposition bases like the orthogonal Haar decomposition [6] or the Rademacher orthogonal decomposition (see definition in "Appendix A.6") [6]. Moreover, for finite energy signals with non-compact support, it is also possible for some specific signals to use a time shift that would guarantee orthogonality. This is the case for the cardinal sine function (see definition in "Appendix A.6" and see Fig. 4a). In this case, the supports are no longer contiguous but they will present an overlap. The block-pulse-based method seems to be ideal for generating K mutually orthogonal signals from a single signal. However, this approach is only suitable for finite energy signal and cannot be used for periodic signals.

To sum up, the literature review shows that OSG can be grouped into three types of analytical methods. The method based on the Hilbert transform leads to the generation of a single orthogonal signal only, the solution being obtained analytically or numerically, often presents singularities in the solution itself. The derivative method can only be used if the signal is derivable and has parity properties, the number of solutions being related to the number of times the signal is derivable. When the generating signal is not symmetric, this method cannot be applied. The block-pulse function method produces as many solutions as desired, as long as the signals have finite energy and compact support. A few rare solutions are possible when the supports are not bounded and no solution is possible for periodic signals.

Furthermore, if we refer to the SIMO-OSG block diagram for electrical application (see Fig. 2a), the SIMO sub-part is not exploited at all since outputs are equal to the input. Moreover, most of the studied signals are periodic signals and the number of orthogonal output signals is limited to two. In order to propose a method that is not limited to periodic signals, whose number of outputs is not limited to two and that allows a greater variety of solutions, new approaches are expected. Finally, since the three methods are always presented independently, a formal framework bringing these methods together is also expected.

Based on this observation and these remarks, the purpose of this article is then to propose in a formal framework an analytical method allowing to generate, from a single signal, as many signals as one wishes while preserving its intrinsic properties: finite energy, derivable, even/odd, oscillating, periodic, etc. In this work, we will voluntarily limit OSG to real signals but it can be easily extended to the case of complex signals.

Subsequently, the formal framework of the proposed method is presented. The main results based on many original examples are presented. A discussion on the advantages and disadvantages is presented, and then, a conclusion and perspectives are proposed.

2 Method and Main Results

In this section, a new framework of orthogonal signal generator (OSG) globalizing the SIMO and MIMO sub-parts reported in Fig. 3 in presented. Several examples will show the originality of the solutions and the interest of basing the analytical calculation exclusively on the use of the input signal $x(t)$.

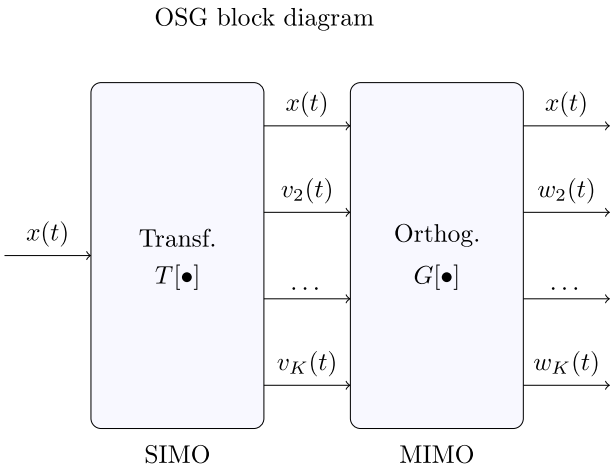

Fig. 3 OSG block diagram of our proposed method. In the SIMO sub-part, the K output signals are obtained from a transformation $T[\bullet]$ defined in Eqs. (1, 6, 10, 14, 17). The K mutually orthogonal signals are obtained with the Gram–Schmidt procedure (a kind of transformation $G[\bullet]$) in the MIMO sub-part. As for OSG represented in Fig. 2, the following relations must be verified: $v_1(t) = w_1(t) = x(t)$

As previously mentioned, it is indeed the design of the SIMO sub-part that is crucial in our solution. As illustrated in Fig. 3, the solution consists in building a dictionary $\mathbf{V}^T = [v_1(t), v_2(t), ..., v_K(t)]$ composed of K non-orthogonal signals $v_k(t)$, by applying a transformation operator from the initial signal $v_1(t) = x(t)$. As we wish a transformation preserving as much as possible the input properties to the output, the following transformations $T_k[\bullet]$ involving time shifts, dilations/compressions will be considered. Afterwards, the orthogonal signals $w_k(t)$ are obtained by applying the Gram–Schmidt (GS) procedure [9, 26, 29] (see ("Appendix A.1") for details) from the non-orthogonal atoms $v_k(t)$. Unlike other methods (QR and SVD decompositions, [29]), the GS approach maintains an analytical framework. In this case, the SIMO dictionary is obtained iteratively as follows:

$$v_k(t) = T_{k-1}\left[v_{k-1}(t)\right], \tag{1}$$

with $v_1(t) = x(t)$.

Using the GS procedure, the calculation of the k-orthogonal atoms $\forall k = \{1, 2, ...\}$ leads to:

$$w_k(t) = T_{k-1}[v_{k-1}(t)] - \sum_{j=1}^{k-1} \rho_{kj} w_j(t). \tag{2}$$

with $w_1(t) = v_1(t) = x(t)$ and with the coefficient

$$\rho_{kj} = \frac{\langle T_{k-1}[v_{k-1}], w_j \rangle_t}{\langle w_j, w_j \rangle_t}, \tag{3}$$

and $< \bullet, \bullet >_t$ defining the scalar product (see the definition in "Appendix A.6").

In order to apply the proposed method to a reduced number of examples, Eq. (2) is voluntarily limited for $K = 3$. Consequently, by using Eqs. (1), (2), (3), the orthogonal atoms become, respectively:

$$\begin{pmatrix} w_1(t) \\ w_2(t) \\ w_3(t) \end{pmatrix} = \begin{pmatrix} 1 & 0 & 0 \\ \gamma_{21} & 1 & 0 \\ \gamma_{31} & \gamma_{32} & 1 \end{pmatrix} \begin{pmatrix} v_1(t) \\ T_1[v_1(t)] \\ T_2[v_2(t)] \end{pmatrix} \tag{4}$$

$$\begin{cases} \gamma_{21} = -\rho_{21}, \\ \gamma_{31} = \rho_{32}\rho_{21} - \rho_{31}, \\ \gamma_{32} = -\rho_{32}. \end{cases} \tag{5}$$

As mentioned earlier, the choice of these transformations $T_k[\bullet]$ depends on the properties of the generating signal and its applications. Consequently, an infinite number of transformations may exist. However, following the literature, we can limit the number of these transformations and their combinations to:

(i) the scale change $v_k(t) = \beta_k v_{k-1}(\beta_k t)$, as in the case in the Haar wavelet basis [6, 19];
(ii) the time shift $v_k(t) = v_{k-1}(t + \tau_k)$ or frequency shift or block pulse, like in the case of the orthogonal sine-cardinal basis used in telecommunications [12];
(iii) the time reversal $v_k(t) = v_{k-1}(-t + \tau_k)$ as proposed in [24]. For the time reversal, a delay must be added, otherwise all $v_k(t) = v_1(-t)$ for odd k and $v_k(t) = v_1(t)$ for even k lead to $w_k(t) = 0 : \forall k > 3$;
(iv) the amplitude shift $v_k(t) = \alpha_k + v_{k-1}(t)$;
(v) the amplification $v_k(t) = \eta_k v_{k-1}(t)$ is not a good choice because it leads to the trivial solution ($w_2(t) = 0$, $w_3(t) = 0$), since $v_{k-1}(t)$ and $v_k(t)$ are not independent;
(vi) all compositions of time shifts, time reversal, amplitude shifts and scale changes can lead to other solutions such as $v_k(t) = \alpha_k + v_{k-1}(-\beta_k t + \tau_k)$.

For the reasons mentioned in Introduction, the operations of derivative and Hilbert transforms will not be considered. Finally, many examples that we found interesting will be presented, so the list of examples is not exhaustive.

2.1 Time-Shift Operation

The time-shift operation is the method of block-pulse functions where the time shifts are fixed manually. However, it does not exist in the form proposed here, i.e. by applying the Gram–Schmidt procedure. The manual method is the most common solution when the signals are compactly supported and is called time-division multiplexing (TDM) in telecommunications [12, 17]. It consists in finding time-shifts that produce disjoint and often contiguous compact supports, as it is the case for signals $w_k(t) = \mathrm{Rect}_T(t - kT)$ where $k \in \mathbb{Z}$.

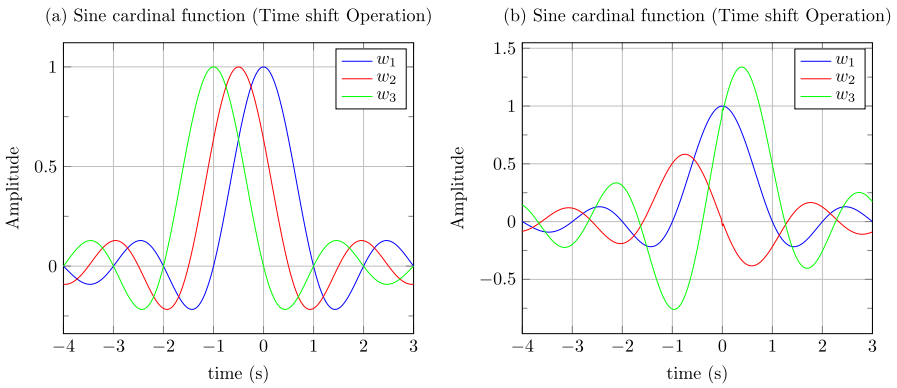

Fig. 4 **a** Orthogonal cardinal sine atoms obtained with time shifts $\tau_1 = -1.0$ s and $\tau_2 = -1.0$ s, and with $\gamma_{21} = -0.005$, $\gamma_{31} = 0.005$ and $\gamma_{32} = -0.005$; the first atom being defined as $v_1(t) = \text{sinc}(t)$. The values of the delays have been chosen so that the $w_k(t)$ are just lagged versions. **b** Innovative orthogonal cardinal sines obtained with time shifts $\tau_1 = -0.4$ s and $\tau_2 = 0.6$ s, and with $\gamma_{21} = -0.759$, $\gamma_{31} = 0.899$ and $\gamma_{32} = -1.191$. The values of the delays were chosen so that the $w_k(t)$ undergoes a temporal shift but also a modification of its amplitude

By applying the equations from (1) to (5) with a transformation based on time shifts, this yields with $\forall k > 1$ and $K = 3$:

$$v_k(t) = T_{k-1}[v_{k-1}(t)] = v_{k-1}(t + \tau_k), \tag{6}$$

with τ_k the time delay and

$$\begin{cases} v_2(t) = T_1[v_1(t)] = v_1(t + \tau_1), \\ v_3(t) = T_2[v_2(t)] = v_2(t + \tau_2) = v_1(t + \tau_3) \end{cases} \tag{7}$$

with $\tau_3 = \tau_1 + \tau_2$.

For $K = 3$, the orthogonal atoms can be written:

$$\begin{cases} w_1(t) = v_1(t), \\ w_2(t) = v_1(t + \tau_1) + \gamma_{21}\, v_1(t), \\ w_3(t) = v_1(t + \tau_3) + \gamma_{32}\, v_1(t + \tau_1) + \gamma_{31}\, v_1(t). \end{cases} \tag{8}$$

The coefficients of Eqs. (3), and (5) are written for $k = 1, 2, 3$:

$$\begin{cases} \gamma_{21} = -\rho(\tau_1), \\ \gamma_{31} = \frac{\rho(\tau_1)\rho(\tau_2) - \rho(\tau_3)}{1 - \rho^2(\tau_1)}, \\ \gamma_{32} = -\frac{\rho(\tau_2) - \rho(\tau_1)\rho(\tau_3)}{(1 - \rho^2(\tau_1))}. \end{cases} \tag{9}$$

with $\rho_{21} = \rho(\tau_1)$, $\rho_{31} = \rho(\tau_3)$ and with $\rho(\tau)$ the autocorrelation coefficient.

Three examples are proposed for constructing an orthogonal basis from the time-shift operation.

(a) The first example proposes the cardinal sine function $v_1(t) = \text{sinc}(t)$ as generator signal (see definition in Table 1). It is an even signal, derivable, of finite energy of non-bounded support and oscillating of period T. Applying Eq. (1), we get $v_2(t) = v_1(t+\tau_1) = \text{sinc}(t+\tau_1)$ and $v_3(t) = v_2(t+(\tau_1+\tau_2)) = \text{sinc}(t-(\tau_1+\tau_2))$. The correlation coefficient is $\rho(\tau) = \text{sinc}(\tau)$ and cancels every $\tau = n \in \mathbb{Z}^*$. When $\tau_1 = -1$ and $\tau_2 = -1$, the orthogonal solutions plotted in Fig. 4a are well known in telecommunications and we have $w_2(t) = \text{sinc}(t+1)$ and $w_3(t) = \text{sinc}(t+2)$. By proposing any value of delay, different from $\tau_1 = -\tau_2$, the solutions are completely new. For example, by proposing $\tau_1 = -0.4$ and $\tau_2 = -0.6$, the signals $w_1(t)$, $w_2(t)$ and $w_3(t)$ obtained provide a much greater overlap than with the classic settings (see Fig. 4b). The price to pay is an amplitude modulation.

(b) The second example proposes the Gaussian function $v_1(t) = \text{e}^{-at^2}$ as generator signal. [4] It is an even signal, derivable, of finite energy, non-bounded and non-oscillating. The correlation coefficient is equal to $\rho(\tau) = \text{e}^{-a\tau^2/2}$. The signals $w_1(t)$, $w_2(t)$ and $w_3(t)$ are depicted in Fig. 5a with $a = 2$, $\tau_1 = 1/4\,\text{s}$, $\tau_2 = -3/4\,\text{s}$, $\rho_{21} = \rho(1/4) = 0.94$, $\rho_{31} = \rho(1/4+3/4) = 0.78$, $\rho(3/4) = 0.57$, $\rho_{32} = -1.38$, $\gamma_{21} = -0.94$, $\gamma_{31} = -2.07$ and $\gamma_{32} = 1.38$. An innovative example is given in Fig. 5b. Note that when the time shift τ tends to zero, the solution obtained for $w_2(t)$ is proportional to the derivative of $w_1(t)$:

$$\lim_{\tau\to 0} w_2(t) = \lim_{\tau\to 0} \tau \frac{w_1(t+\tau) - \rho_{21}(\tau) w_1(t)}{\tau} = \lim_{\tau\to 0} \tau \frac{w_1(t+\tau) - w_1(t)}{\tau} = \tau \frac{\text{d}w_1(t)}{\text{d}t},$$

with $\lim_{\tau\to 0} \rho_{21}(\tau) = 1$. In the present example the derivative is expressed by $\frac{\text{d}w_1(t)}{\text{d}t} = \frac{1}{\tau} w_2(t)$.

(c) The third example proposes the periodic rectangular signal of period T as generator signal. It is an odd, not derivable signal due to singularities and of finite average power. The correlation coefficient is equal to $\rho(\tau) = \text{Tri}_T * \text{III}_{2T}(\tau)$ where $*$ is the convolution operation, Tri_T is the triangular signal and $\text{III}_T(t)$ is the Dirac comb (see the three definitions in "Appendix A.6"). The signals $w_1(t)$, $w_2(t)$ and $w_3(t)$ are plotted in Fig. 6 with $\tau_1 = -0.15$ s, $\tau_2 = -0.30$ s, $T = 1$ s, $\gamma_{21} = -0.400$, $\gamma_{31} = 0.857$, $\gamma_{32} = -0.143$. The solution proposed in Fig. 6a) is an innovative and alternative solution to methods providing singularities like the derivative and the Hilbert transform. Another solution is presented in Fig. 6b) with $\tau_1 = -0.25$ s, $\tau_2 = -0.25$ s, $\gamma_{21} = 0$, $\gamma_{31} = 1$, $\gamma_{32} = 0$, the first atom being defined by $v_1(t) = \text{sign}(\sin(\omega t))$ with $T = 1$ s, the sign function is defined in "Appendix A.6".

At this level, several remarks can be expressed. First of all, whatever the type of signals considered (finite energy and finite average power), the method always provides at least one solution. For finite energy signals, solutions for $K > 2$ are possible

[4] The Gaussian function being frequently used in signal processing, it seemed important to propose several analytical solutions other than those obtained by the derivative method which is a particular solution of our approach when the delay approaches zero.

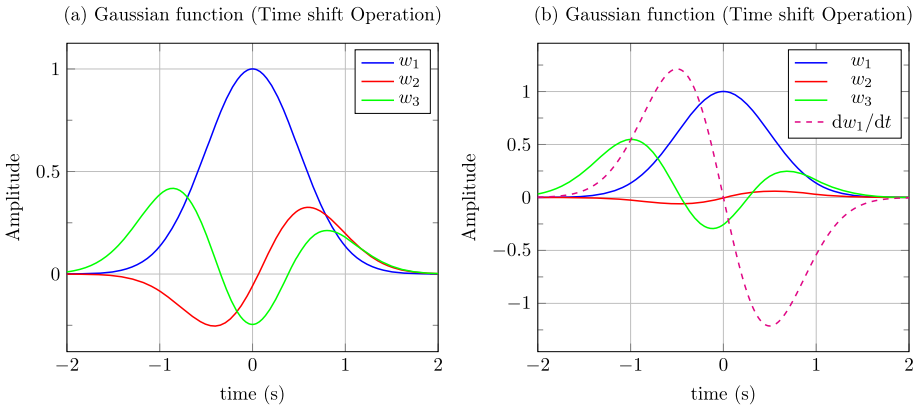

Fig. 5 **a** Orthogonal Gaussian atoms obtained with time shifts $\tau_1 = 1/4$ s and $\tau_2 = -3/4$ s, and with $a = 2$, $\rho_{21} = \rho(1/4) = 0.94$, $\rho_{31} = \rho(1/4 + 3/4) = 0.78$, $\rho(3/4) = 0.57$, $\rho_{32} = -1.38$, $\gamma_{21} = -0.94$, $\gamma_{31} = -2.07$ and $\gamma_{32} = 1.38$; the first atom being defined by $v_1(t) = \mathrm{e}^{-at^2}$. **b** Innovative orthogonal Gaussian atoms obtained with time shifts $\tau_1 = 0.05$ s, $\tau_2 = -3/4$ s, $a = 2$, $\rho_{21} = 1.00$, $\rho_{31} = 0.61$, $\rho(3/4) = 0.57$, $\rho_{32} = -8.28$, $\gamma_{21} = -1.00$, $\gamma_{31} = -8.88$ and$\gamma_{32} = 8.29$, the first atom being defined by $v_1(t) = \mathrm{e}^{-at^2}$. The derivative of the Gaussian function is reported in dashed line with $\tau = -1/4$ meaning that the derivative is (-4) times higher than $w_2(t)$

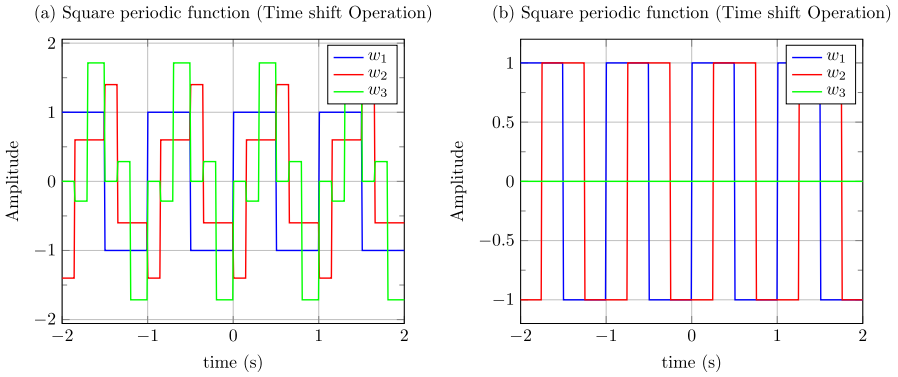

Fig. 6 **a** Innovative orthogonal atoms obtained with time shifts $\tau_1 = -0.15$ s, $\tau_2 = -0.15$ s, $\gamma_{21} = -0.400$, $\gamma_{31} = 0.857$, $\gamma_{32} = -0.143$, the first atom being defined by $v_1(t) = \mathrm{sign}(\sin(\omega t))$ with $T = 1$ s. **b** Orthogonal atoms obtained with time shifts $\tau_1 = -0.25$ s, $\tau_2 = -0.25$ s, $\gamma_{21} = 0$, $\gamma_{31} = 1$, $\gamma_{32} = 0$, the first atom being defined by $v_1(t) = \mathrm{sign}(\sin(\omega t))$ with $T = 1$ s

with an adequate adjustment of the time delays. As for the periodic signal, note that when the generator signal is a sinusoidal signal $v_1(t) = \cos\left(\frac{2\pi}{T}t\right)$, the correlation coefficient $\rho(\tau) = \cos\left(\frac{2\pi}{T}\tau\right)$ is periodic too and the atoms obtained for $K > 2$ are null, for any chosen delays values. On the other hand, the periodic signal reported in Fig. 6a is completely novel. Finally, whatever the nature of the signal for which $\lim_{\tau\to 0}\rho_{21}(\tau) \to 1$ is verified and with $K = 2$, the solution obtained is proportional to the derivative.

2.2 Scaling Operation

The scaling operation is inspired by orthogonal wavelet based decompositions, such as the Haar base [6, 19]. However, in the case of the scaling operation proposed here, no particular property is imposed and any generative signal can be used. In the case of scaling, Eq. (1) becomes:

$$v_k(t) = T_{k-1}[v_{k-1}(t)] = \beta_k v_{k-1}(\beta_k t), \tag{10}$$

where β_k is the scaling factor. With $k > 1$ and $K = 3$, it comes:

$$\begin{cases} v_2(t) = T_1[v_1(t)] = v_1(\beta_1 t), \\ v_3(t) = T_2[v_2(t)] = v_2(\beta_2 t) = v_1(\beta_3 t) \end{cases} \tag{11}$$

with $\beta_3 = \beta_1 \beta_2$.

For $K = 3$, the orthogonal atoms are written:

$$\begin{cases} w_1(t) = v_1(t), \\ w_2(t) = \beta_1 v_1(\beta_1 t) + \gamma_{21}\, v_1(t), \\ w_3(t) = \beta_3 v_1(\beta_3 t) + \gamma_{32}\, \beta_1 v_1(\beta_1 t) + \gamma_{31}\, v_1(t). \end{cases} \tag{12}$$

The coefficients of Eqs. (3) and (4) are written for $K = 3$:

$$\begin{cases} \gamma_{21} = -\rho(\beta_1), \\ \gamma_{31} = \frac{\rho(\beta_1)\rho(\beta_2) - \rho(\beta_3)}{1 - \rho^2(\beta_1)/\beta_1}, \\ \gamma_{32} = -\frac{\beta_1 \rho(\beta_2) - \rho(\beta_1)\rho(\beta_3)}{(\beta_1 - \rho^2(\beta_1))}. \end{cases} \tag{13}$$

with $\rho_{21} = \rho(\beta_1)$, $\rho_{31} = \rho(\beta_3)$.

Three examples are proposed to build an orthogonal basis from the scaling operation.

(a) The first example proposes the rectangular function as generator signal: $v_1(t) = \mathrm{Rect}_T(t - T/2)$, $\mathrm{Rect}_T(t)$ being the rectangular function defined in "Appendix A.6". It is a finite energy signal with compact support widely used in telecommunications (block-pulse method). The scale coefficient is equal to:

$$\rho(\beta) = \begin{cases} \beta \ \forall 0 \leq \beta \leq 1, \\ 1 \ \forall \beta > 1. \end{cases}$$

The orthogonal signals $w_1(t)$, $w_2(t)/\beta_2$ and $w_3(t)/\beta_3$ of duration $T = 1$ s, obtained with $\beta_2 = 1/2$, $\beta_3 = 1/3$, $\rho_{21} = 1/2$, $\rho_{31} = 1/6$, $\rho_{32} = 1/3$, $\gamma_{21} = -1/2$, $\gamma_{31} = 0$ and $\gamma_{32} = -1/3$ are reported in Fig. 7a. The signals obtained are of disjoint and contiguous supports. For another settings, the orthogonal rectangular atoms $w_1(t)$, $w_2(t)/\beta_2$ and $w_3(t)/\beta_3$ are obtained by scaling with $T = 2.5$ s, $\beta_2 = 3/2$, $\beta_3 = 1/2$, $\rho_{21} = 1$, $\rho_{31} = 3/4$, $\rho_{32} = 0$, $\gamma_{21} = -1$, $\gamma_{31} = -3/4$ and $\gamma_{32} = 0$ are reported in Fig. 7b. Orthogonal signals are no longer disjoint.

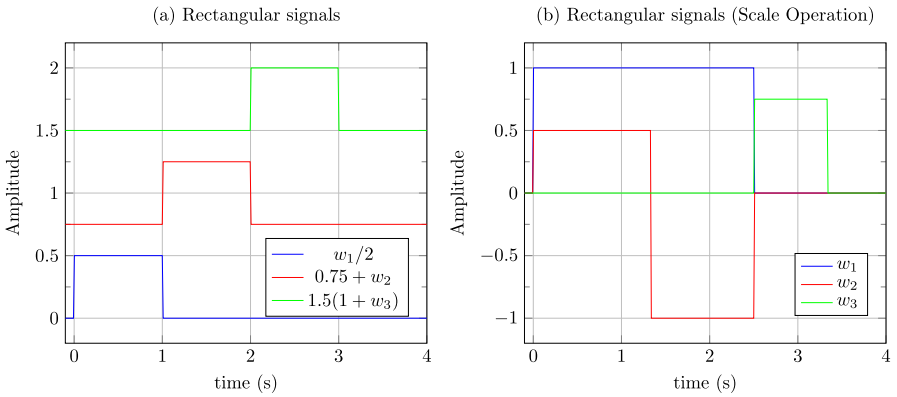

Fig. 7 **a** Orthogonal rectangular atoms $w_1(t)$, $w_2(t)/\beta_2$ and $w_3(t)/\beta_3$ obtained by a scale change with $T = 1$ s, $\beta_1 = 1/2$, $\beta_2 = 1/3$, $\rho_{21} = 1/2$, $\rho_{31} = 1/6$, $\rho_{32} = 1/3$, $\gamma_{21} = -1/2$, $\gamma_{31} = 0$ and $\gamma_{32} = -1/3$; the first atom being defined by $w_1(t) = v_1(t) = Rect_T(t - T/2)$. **b** Innovative orthogonal atoms $w_1(t)$, $w_2(t)/\beta_1$ and$w_3(t)/\beta_2$ obtained by a scale change with $T = 2.5$ s, $\beta_1 = 3/2$, $\beta_2 = 1/2$, $\rho_{21} = 1$, $\rho_{31} = 3/4$, $\rho_{32} = 0$, $\gamma_{21} = -1$, $\gamma_{31} = -3/4$ and$\gamma_{32} = 0$; the first atom being defined by $w_1(t) = v_1(t) = \text{Rect}_T(t - T)$

(b) The second example proposes the cosine function as generator signal: $v_1(t) = \cos\left(\frac{2\pi}{T}t\right)$. It is a derivable, even and oscillating signal of period T and finite average power. The scale coefficient is equal to

$$\rho(\beta) = \beta\,\text{sinc}(2\pi(\beta + 1)) + \beta\,\text{sinc}(2\pi(\beta - 1)).$$

It is an even function where the maximum values are located in $\beta = \pm 1$, and the zero crossings are located every $\beta = \{0, \pm 1/2, \pm 3/2, ...\}$. An example of the signals $w_1(t)$, $w_2(t)$ and $w_3(t)$ is reported in Fig. 8a for a duration of 4 s, with $f = 4$ Hz, $\beta_1 = 3/4$, $\beta_2 = 5/4$. We notice here that the orthogonal signals obtained $w_2(t)$ and $w_3(t)$ are of the same nature as the generator signal, they present however an amplitude modulation.

(c) The third example proposes as generator signal the modulated exponential function: $v_1(t) = \cos(\omega t)\mathrm{e}^{-at}u(t)$, where $u(t)$ is the Heaviside function defined in "Appendix A.6". It is a derivable, oscillating signal of period T, causal and of finite energy with unbounded support. The scale function is

$$\rho(\beta) = \left(\frac{2\beta/(\beta + 1)}{2 + (\omega/a)^2}\right)\left(1 + \frac{1 + (\omega/a)^2}{1 + \left(\frac{\omega(\beta-1)}{a(\beta+1)}\right)^2}\right).$$

An example of the signals $w_1(t)$, $w_2(t)$ and $w_3(t)$ is depicted in Fig. 8b for a duration of 8 s, with $\beta_2 = 4$, $\beta_3 = 3/2$, $a = 1/3$, $\omega = 3a$, $\gamma_{31} = -0.058$, $\gamma_{32} = -0.746$ and $\gamma_{21} = -0.403$. The obtained orthogonal signals present the same properties of the generator signal, i.e. derivable, causal and of finite energy with non-bounded support, only the frequency is modified.

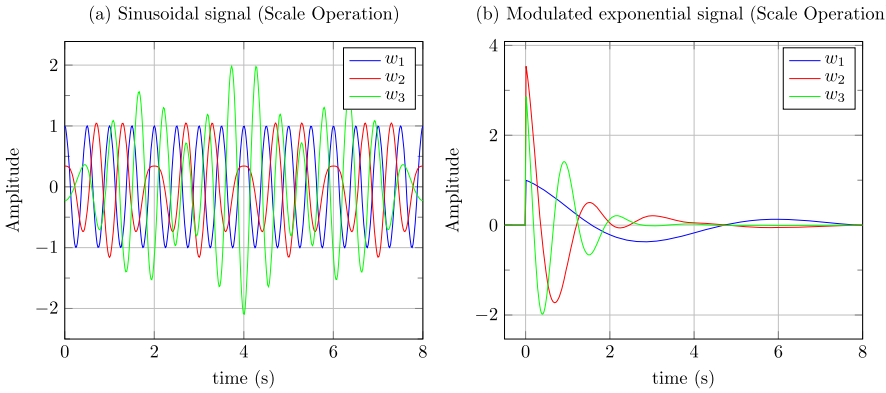

Fig. 8 **a** Orthogonal atoms obtained scale change with $\beta_1 = 3/4$ and$\beta_2 = 5/4$, $\gamma_{21} = -0.409$, $\gamma_{31} = -0.543$, $\gamma_{32} = -0.830$; the first atom being defined by $v_1(t) = \cos(2\pi f t)$ for $f = 4$ Hz. **b** Orthogonal atoms obtained with $w_1(t) = \cos(2\pi t/T)\mathrm{e}^{-at}u(t)$ with $\beta_2 = 4$, $\beta_3 = 3/2$, $a = 1/3$, $\omega = 3a$, $\gamma_{31} = -0.058$, $\gamma_{32} = -0.746$ and $\gamma_{21} = -0.403$

For this type of transformation, there are no particular restrictions, as the orthogonal signals obtained present similar properties if compared with the generator signal. Note that for the cosine generator signal, if there were only 2 distinct solutions in the case of the time-shifting operation, for the scaling operation, there are as many solutions as necessary. It should also be noted that the solutions obtained correspond to sinusoidal signals modulated in amplitude, because of the beat phenomenon between the generator signal of frequency f and the orthogonal signal of frequency βf.

2.3 Time-Reversal Operation

The time-reversal operation proposed here echoes the method proposed by [24] in order to orthogonalize linearly frequency modulated signals (sweep). The time-reversal operation, which allows us to obtain the atom $v_{k-1}(t)$ from an atom $v_k(t)$, is defined $\forall k > 1$ and $K = 3$ by

$$v_k(t) = T_k[v_{k-1}(t)] = v_1((-1)^k t + \tau_k).$$

The introduction of the delay τ_k combined with the time reversal allows to increase the calculation of the number of atoms. Indeed for $\tau_1 = \tau_2 = 0$, $v_2(t) = v_1(-t)$ and $v_3(t) = v_1(t)$, $\rho_{31} = 1$, $\gamma_{31} = -1$ and $\rho_{32} = 0$, results in $w_3(t) = 0$. For $K = 3$, this yields:

$$\begin{cases} v_2(t) = T_1[v_1(t)] = v_1(-t + \tau_1), \\ v_3(t) = T_2[v_2(t)] = v_2(t + \tau_2) = v_1(-t + \tau_3) \end{cases} \tag{14}$$

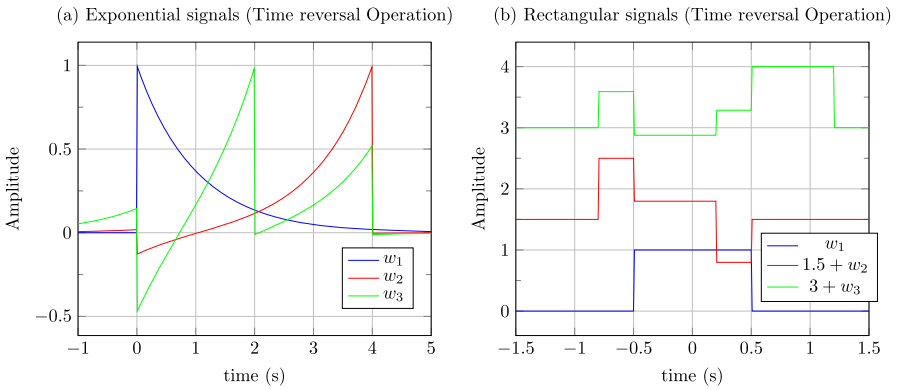

Fig. 9 **a** Orthogonal atoms obtained for $w_1(t) = \mathrm{e}^{-at}u(t)$ with $a = 1$, $\tau_1 = 4$, $\tau_2 = 2$, $\gamma_{21} = -0.147$, $\gamma_{31} = -0.619$ and $\gamma_{32} = 0.533$. **b** Orthogonal atoms obtained for $w_1(t) = \mathrm{Rect}_T(t)$ with $T = 1$ s, $\tau_1 = 0.2$, $\tau_2 = -0.4$, $\gamma_{21} = -0.702$, $\gamma_{31} = -0.714$ and $\gamma_{32} = 0.590$

with $\tau_3 = \tau_1 - \tau_2$. Coefficients are defined by:

$$\begin{cases} \gamma_{21} = -\rho_{21} \\ \gamma_{31} = \frac{\nu_{32}\rho_{21} - \rho_{31}}{1-\rho_{21}^2}, \\ \gamma_{32} = -\frac{\nu_{32} - \rho_{21}\rho_{31}}{(1-\rho_{21}^2)}, \end{cases} \tag{15}$$

with $\rho_{21} = C(\tau_1)/\|w_1\|^2$, $\rho_{31} = C(\tau_3)/\|w_1\|^2$ with $\rho(\tau) = C(\tau)/\|w_1\|^2$ and where $C(\tau) = v_1(\tau) * v_1(\tau)$ is the auto-convolution function and with $\|w_2\|^2 = \|w_1\|^2(1 - \rho_{21}^2)$ and $\nu_{32} = \frac{R_{32}(\tau_3 - \tau_1)}{\|w_1\|^2}$ where $R_{32}(\tau_3 - \tau_1)$ is the cross-correlation function between $v_3(t)$ and $v_2(t)$.

For $K = 3$, the orthogonal atoms write:

$$\begin{cases} w_1(t) = v_1(t), \\ w_2(t) = v_1(-t + \tau_1) + \gamma_{21}\, v_1(t), \\ w_3(t) = v_1(-t + \tau_3) + \gamma_{32}\, v_1(-t + \tau_1) + \gamma_{31}\, v_1(t). \end{cases} \tag{16}$$

Two examples are proposed and reported in Fig. 9:

- The generator signal is $v_1(t) = \mathrm{e}^{-at}u(t)$. It is a derivable, causal, finite energy signal with unbounded support. The coefficients are written $\rho_{21} = \rho(\tau_1)$, $\rho_{31} = \rho(\tau_3)$ with $\rho(\tau) = 2a\tau\mathrm{e}^{-a\tau}u(\tau)$, $\rho_{32} = \mathrm{e}^{-a|\tau_3 - \tau_1|}$ and $a = 1$. Orthogonal signals are reported in Fig. 9a; Note that for $\tau_1 \leq 0$, we obtain the anti-causal solution for $w_2(t) = \mathrm{e}^{at}u(-t)$.
- The generator signal is $v_1(t) = \mathrm{Rect}_T(t)$ with $T = 1$ s. It is note derivable due to discontinuities at $|t| = T/2$ and it is a finite energy signal with compact support. The auto-convolution is $C(\tau) = Tri_T(\tau)$. Parameters are $\tau_1 = 0.2$, $\tau_2 = -0.4$, $\gamma_{21} = -0.702$, $\gamma_{31} = -0.714$ and $\gamma_{32} = 0.590$. Orthogonal signals are reported in Fig. 9b.

Note that the orthogonal signals shown in Fig. 9 are completely new. In practice, time-reversal signals can be obtained using memories.

2.4 Amplitude Shift Operation

For the 3 previous operations, the energy nature of the signal has not been strongly modified. Here, the amplitude shift operation which consists in adding a DC component to the generating signal will transform a finite energy signal into a finite average power signal, the nature of the finite average power generating signals will not be changed. If this point is not a constraint, then from the atom $v_{k-1}(t)$, the atom $v_k(t)$ is obtained $\forall k > 1$ and $K = 3$ by:

$$v_k(t) = T_{k-1}[v_{k-1}(t)] = \alpha_k + v_{k-1}(t), \tag{17}$$

where α_k is the shift amplitude.

For $K = 3$, Eq. (1) becomes:

$$\begin{cases} v_2(t) = T_1[v_1(t)] = \alpha_1 + v_1(t), \\ v_3(t) = T_2[v_2(t)] = \alpha_1 + v_2(t) = \alpha_3 + v_1(t), \end{cases} \tag{18}$$

with $\alpha_3 = \alpha_1 + \alpha_2, \alpha_1,\ \alpha_2, \alpha_3\ \in \mathbb{R}^*$. For $K = 3$, the orthogonal atoms being:

$$\begin{cases} w_1(t) = v_1(t), \\ w_2(t) = \alpha_1 + v_1(t) + \gamma_{21} v_1(t), \\ w_3(t) = (\alpha_3 + v_1(t)) + \gamma_{32}(\alpha_1 + v_1(t)) + \gamma_{31} v_1(t). \end{cases} \tag{19}$$

Note that orthogonal signals can be expressed simply as $w_k(t) = \eta_k + \mu_k v_1(t)$. The coefficients are expressed as:

$$\begin{cases} \gamma_{21} = -\rho(\alpha_1) \\ \gamma_{31} = \frac{\nu + \rho(\alpha_1+\alpha_3) - \rho(\alpha_1)\rho(\alpha_3)}{(1-\rho(\alpha_1))}, \\ \gamma_{32} = \frac{\nu + \rho(\alpha_1+\alpha_3) - \rho(\alpha_1)\rho(\alpha_3)}{\rho(\alpha_1)(1-\rho(\alpha_1))}, \end{cases} \tag{20}$$

with $\nu = \frac{\alpha_1 \alpha_3 c}{\|v_1\|^2}$ where c is a constant of integration, and with $\rho(\alpha) = 1 + \alpha \frac{\overline{v_1}}{\|v_1\|^2}$, $\rho_{21} = \rho(\alpha_1)$, $\rho_{31} = \rho(\alpha_3)$, where $\overline{v_1(t)} = \langle v_1, 1 \rangle_t$.

Two examples are proposed to build an orthogonal basis from the amplitude shift operation.

(a) The first proposed example has as generator signal the exponential signal: $v_1(t) = e^{-at}u(t)$. It is a derivable, causal and finite energy signal with non-bounded support. The coefficient $\rho(\alpha)$ is written: $\rho(\alpha) = 2\alpha + 1$. The orthogonal atoms $w_1(t)$, $w_2(t)$, $w_3(t)$ obtained by amplitude shift $\alpha_1 = 1/4$ and $\alpha_2 = 1/4$ are plotted in Fig. 10a with $a = 1$, $\gamma_{21} = -1.491$, $\gamma_{31} = -7.701$, and $\gamma_{32} = 3.835$. Although the generating signal is causal, the atoms $w_2(t)$, $w_3(t)$ are no longer causal due to the amplitude shift;

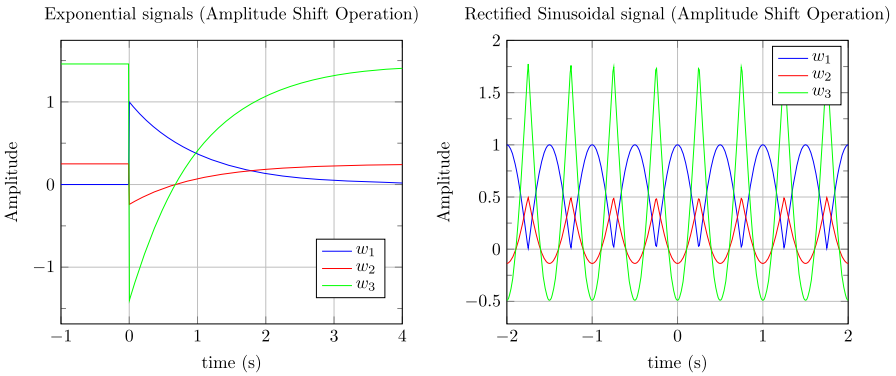

Fig. 10 **a** Orthogonal atoms obtained by amplitude shift, $\alpha_1 = 1/4$, $\alpha_2 = 1/4$, the first atom being defined by $w_1(t) = \mathrm{e}^{-at}u(t)$, with $a = 1$, $\gamma_{21} = -1.491$, $\gamma_{31} = -7.701$ and $\gamma_{32} = 3.835$. **b** Orthogonal atoms obtained by amplitude shift $\alpha_1 = 1/2$, $\alpha_3 = 3/4$. The first atom being defined by $w_1(t) = |\cos(2\pi f t)|$, with $f = 1$ Hz, $\gamma_{21} = -1.636$, $\gamma_{31} = -5.379$ and $\gamma_{32} = 2.093$

(b) The second example proposed has for generator signal the absolute value function of the cosine signal: $v_1(t) = |\cos(2\pi f t)|$. It is not derivable over $\mathbb{R}$, even, periodic signal of period $T = 1/2$ s of finite average power. The coefficient $\rho(\alpha)$ is equal to $\rho(\alpha) = \alpha\left(\frac{8}{\pi - 2}\right) + 1$. An illustration of the orthogonal atoms $w_1(t)$, $w_2(t)$ and $w_3(t)$ is reported in Fig. 10b with $f = 1$Hz, $\alpha_1 = 1/2$, $\alpha_3 = 3/4$, $\gamma_{21} = -1.636$, $\gamma_{31} = -5.379$ and $\gamma_{32} = 2.093$. Note that the all input–output properties are preserved.

This transformation seems more adapted to signals with finite average power since the added component α_k is itself of finite average power. However, for finite energy signals, we could replace α_k by $\alpha_k \mathrm{Rect}_T(t)$ and by other elementary signals.

2.5 Note: Numerical Calculation

Note that in all cases, it is always possible to compute numerically the different scalar products from Eq. (3). In the case of digital signals or digitized continuous signals, the calculation of the $\gamma_{k,j}$ coefficients (from Eq. 5) is obtained by numerically calculating the $\rho_{k,j}$ coefficients from the digital versions of the signals $\mathbf{v}_k^T = [v_k(1), ..., v_k(N)]$, N being the number of points composing the vector $\mathbf{v}_k^T$. For example for the calculation of $\rho_{2,1}$ we get: $\rho_{2,1} = \frac{\mathbf{v}_1^T \mathbf{v}_2}{\mathbf{v}_1^T \mathbf{v}_1}$ where $\mathbf{v}_1^T = [v_1(1), ..., v_1(N)]$ and $\mathbf{v}_2^T = [v_2(1), ..., v_2(N)]$ are the numerical versions of signals $v_1(t)$ and $v_2(t)$.

For example by applying a transformation operator from the composition of operations $T_k[v_{k-1}] = \alpha_k + \beta_k v_1((-1)^k \beta_k t + \tau_k)$ and applied to the generating signal $v_1(t) = t^2 \mathrm{e}^{-at}\cos(2\pi f t^2)$ representing a linear frequency modulation (see Matlab code in "Appendix A.5"). In this case, the too complex analytical form is not accessible whereas its numerical calculation is possible and leads to the results reported in Fig. 11 with $K = 3$.

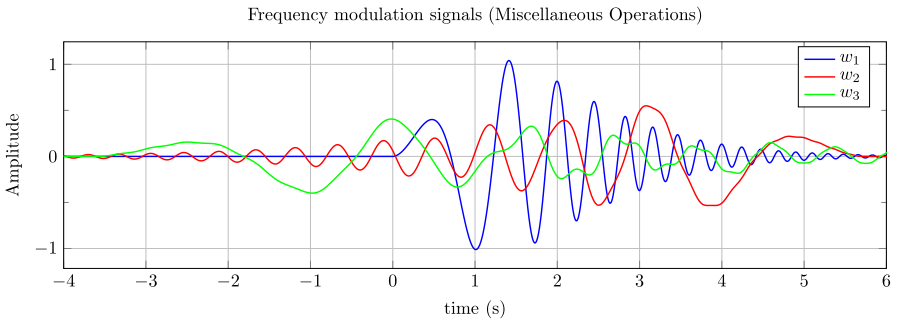

Fig. 11 Orthogonal atoms obtained numerically from the transformation $T_k[v_1] = \alpha_k + \beta_k v_1((-1)^k \beta_k t + \tau_k)$ and for the generator signal $v_1(t) = t^2 e^{-at} \cos(2\pi f t^2)$ with $K = 3$. The sampling frequency is of $F_s = 1000$ Hz

3 Discussions and Conclusion

In this paper, a new OSG structure composed of two parts was proposed. A SIMO sub-part exploits transformations $T[\bullet]$, and a MIMO sub-part uses the Gram–Schmidt procedure (a kind of transformation $G[\bullet]$). The method provides a formal framework that provides directly usable analytical solutions through the calculation of coefficients $(\rho_{k,j}, \gamma_{k,j})$ and the setting of parameters $(\tau_k, \beta_k, \alpha_k)$ depending of the transformation used. The proposed method can be used both from analytical and digital framework. Moreover, the obtained orthogonal signals are novel for most of them and their properties are very similar to the only available signal $x(t)$. This could be an important advantage for practical applications. Furthermore, these solutions could probably not have been obtained from traditional methods. To show the applicability of the presented approach, two families of signals have been studied: finite energy signals and finite average power signals.

Based on existing orthogonal decompositions from purely mathematical approaches, four elementary signal processing operations have been proposed: time shifts, scaling, time reversal and amplitude shifts. We then built a base of orthogonal atoms by proposing a generator signal at the k iteration of the process which follows the same model: $v_k(t) = T_k[v_{k-1}]$. In this case, the transformation is identical throughout the process. However, other transformations different at each iteration can also be used, such as $v_2(t) = T_2[v_1] = v_1(t + \tau_1)$ and $v_3(t) = T_3[v_2] = v_2(\beta_2 t) = v_1(\beta_2 t + \tau_1)$. Although only linear transformations have been used, this work can be extended to the use of nonlinear transformations, such as $v_2(t) = T_2[v_1] = v_1^{1/2}(t)$ and $v_3(t) = T_3[v_2] = v_2(\beta_2 t) = v_1^{1/3}(t)$. In this case, the difficulty lies in the analytical calculation of the coefficients γ_{kj} and ρ_{kj}.

Another interesting point in the presented approach is that the different elements resulting from the α_k, β_k and τ_k transformations can be calculated randomly from a list of pre-established values or not. For example, in a communication protocol, the time shift τ_k could be carrier frequencies archived in the configuration system and made secret to the users. This may enhance security and privacy.

Finally, the strength of the proposed method lies in its simplicity, its efficiency and it offers an analytical framework that can be easily replaced by a numerical one.

The main drawback of the presented method is that for some transformations and generator signals, the analytical formulation becomes of difficult application. In these particular cases, a numerical implementation may be considered.

Finally, the real-time aspect was not taken into account in this work, and it could constitute a new track to explore.

Declarations

Competing Interests Conflict of interest: none.

Appendix A. Appendix

Appendix A.1. Gram–Schmidt (GS) procedure

The Gram–Schmidt (GS) procedure [9, 20, 26, 29] is used to make orthogonal an input dictionary $\mathbf{V}^T = [v_1(t), v_2(t), ..., v_K(t)]$ composed of K signals, the output dictionary $\mathbf{W}^T = [w1(t), w_2(t), ..., w_K(t)]$ being composed of K mutually orthogonal signals. The orthogonal signals $w_k(t)$ are obtained iteratively using the following relationship for k ranging from 1 to K:

$$w_k(t) = v_k(t) - \sum_{j=1}^{k-1} \rho_{kj} w_j(t)$$

with the coefficient

$$\rho_{kj} = \frac{\langle v_k, w_j \rangle_t}{\langle w_j, w_j \rangle_t},$$

and $< \bullet, \bullet >_t$ defining the scalar product in the time domain ranging from t_1 to t_2. Note however that our approach is not limited to signals, the method can also be applied to spectra [12] and in this case, the scalar product will relate to the variable f over an integration space ranging from f_1 to f_2. As an illustration, a signal approximation example using the GS procedure is reported in Appendix A.2.

Appendix A.2. Signal Approximation

As an illustration, let us consider the signal approximation issue for which the signal to be approximated is $x(t) = \text{Rect}_T(t - T/2)$. The signal $x(t)$ is a non-oscillating signal of finite energy, of compact support with 2 discontinuities at $t = 0$ and $t = T = 1$ s. This signal can be decomposed into a dictionary whose generative signal is $v_k(t) = \exp(-kt)u(t)$, $u(t)$ being the Heaviside signal (see Fig. 12). In this case, the different

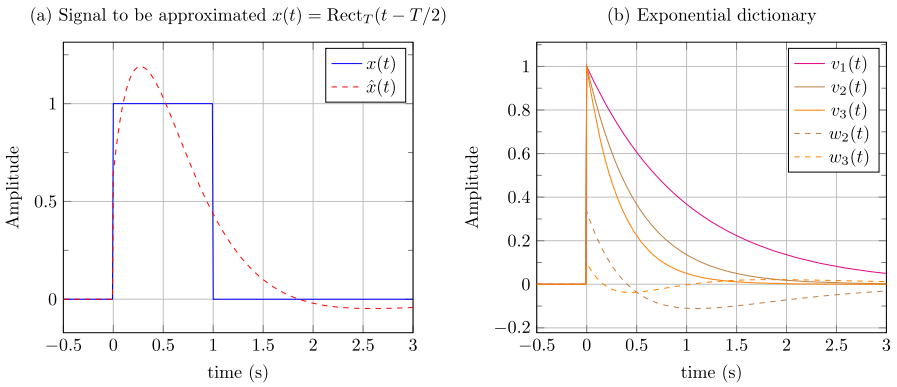

Fig. 12 **a** Rectangular signal $x(t)$ to be approximated and its approximation $\hat{x}(t)$ (in dashed line). **b** Exponential dictionary with $v_1(t), v_2(t), v_3(t)$ and its orthogonal basis $w_1(t) = v_1(t), w_2(t), w_3(t)$ (dashed line)

scalar products are calculated from $t = 0$ to $+\infty$. With $K = 3$ and after calculation, the approximated signal is a linear combination $\hat{x}(t) \approx -1.31v_1(t) + 9.58v_2(t) - 7.64v_3(t)$ and the mean square error is $MSE = 0.029$. From the input dictionary $\mathbf{V}^T = [v_1(t), v_2(t), v_3(t)]$, we construct a dictionary of mutually orthogonal signals $\mathbf{W}^T = [w_1(t), w_2(t), w_3(t)]$. For $K = 3$, the approximated signal $\hat{x}(t)$ is a linear combination: $\hat{x}(t) \approx 1.27w_1(t) + 0.36w_2(t) - 7.64w_3(t)$ and the mean square error is $MSE = 0.029$. In this case, $w_1 = v_1(t)$, $w_2 = v_2(t) - \frac{2}{3}v_1(t)$, $w_3 = v_3(t) - \frac{6}{5}v_2(t) + \frac{3}{10}v_1(t)$, $v_1(t) = \exp(-t)u(t)$, $v_2(t) = \exp(-2t)u(t)$ and $v_3(t) = \exp(-3t)u(t)$. Whatever the approximation (via $v_k(t)$ or $w_k(t)$), the mean square error from the original signal is significant ($MSE = 0.029$). This deviation could be reduced by increasing the number K of signals used or by changing the base with a more adapted generative signal.

Appendix A.3. Derivative-Based Method

Let us show $\langle v_e, \dot{v}_e \rangle = 0$. If the real signal $v(t) = v_e(t)$ is even (or odd $v(t) = v_o(t)$), then the derivative of the signal $y(t) = \dot{v}_e(t)$ is orthogonal: $\langle v_e, \dot{v}_e \rangle = 0$. To prove it, one could just show that $y(t)$ is odd, i.e. $-y(t) = y(-t)$:

$$y(t) = \dot{v}_e(t) = \lim_{h \to 0} \frac{v_e(t+h) - v_e(t)}{h}, \tag{A.1}$$

$$y(-t) = \lim_{h \to 0} \frac{v_e(-t+h) - v_e(-t)}{h}.$$

As $v(t)$ is even, we verify that $v_e(t) = v_e(-t)$ and $v_e(t-h) = v_e(-t+h)$. Hence,

$$y(-t) = \lim_{h \to 0} \frac{v_e(t-h) - v_e(t)}{h},$$

and if we impose $\tau = t - h$, this yields:

$$\lim_{h\to 0} \frac{v_e(\tau) - v_e(\tau + h)}{h} = \lim_{h\to 0} -\frac{v_e(\tau + h) - v_e(\tau)}{h} = -y(\tau).$$

By replacing $t \to \tau$, it comes

$$y(t) = \lim_{h\to 0} -\frac{v_e(t + h) - v_e(t)}{h} = -y(t). \tag{A.2}$$

Consequently, as $y(t) = \dot{v}_e(t)$ is odd and $v_e(t)$ is even, then $\langle v_e, \dot{v}_e \rangle = 0$. QED (quod erat demonstrandum).

Appendix A.4. Hilbert Transform

(a) Let us show $HT[HT[v_1(t)]] = HT[\tilde{v}_1(t)] = -v_1(t)$ where $HT[\bullet]$ refers to the Hilbert Transform. Let us consider $v_1(t)$ and $\tilde{v}_1(t) := HT[v_1(t)]$. By definition, the spectrum of $v_1(t)$ is: $FT[\tilde{v}_1(t)] = \tilde{V}_1(f)$ ($FT[\bullet]$ refers to the Fourier transform) and the spectrum of $\tilde{v}_1(t)$ is:

$$\tilde{V}_1(f) := (-j) \cdot \operatorname{sgn}(f) V_1(f).$$

By multiplying the right and left terms by $(-j)\operatorname{sgn}(f)$, it comes:

$$(-j)\operatorname{sgn}(f) \times \tilde{V}_1(f) = (-j)\operatorname{sgn}(f)(-j)\operatorname{sgn}(f) V_1(f) = -V_1(f).$$

With $\operatorname{sgn}^2(f) = 1$, it comes:

$$FT^{-1}[(-j)\operatorname{sgn}(f)\tilde{V}_1(f)] = FT^{-1}[-V_1(f)]$$

$$HT[\tilde{v}_1(t)] = -v_1(t).$$

QED.

(b) Let us show $v_1(t) \perp \tilde{v}_1(t)$, i.e. $< v_1, \tilde{v}_1 >_t = 0$. Let us consider $v_1(t)$ is real. By virtue of the product theorem, it comes:

$$< v_1, \tilde{v}_1 >_t = < V_1, \tilde{V}_1 >_f$$

$$< V_1, \tilde{V}_1 >_f = \int V_1(f) \times \tilde{V}_1(f) df = \int V_1(f) \times (-j)\, sgn(f) V_1(f) df$$

$$< V_1, \tilde{V}_1 >_f = (-j) \int V_1^2(f) sgn(f) df.$$

As $v_1(t)$ is real, $V_1(f)$ is even. As $\text{sgn}(f)$ is odd then $V_1(f) \times \text{sgn}(f)$ is odd too and $\int V_1^2(f)\text{sgn}(f)df = 0$ that implies $< V_1, \tilde{V}_1 >_f = 0 < v_1, \tilde{v}_1 >_t$, QED.

Appendix A.5. Matlab Code of Example from Fig. 11

```
clear;clc;close all;N=10000;
Duration=14;t=(-Duration/2:Duration/(N-1):Duration/2);
f=0.5;a=1.6;
beta1=0.54;beta2=0.71;beta3=beta1*beta2;
tau1=3.1;tau2=-1.7;
tau3=tau1+tau2;
alpha1=0;alpha2=0;alpha3=alpha1+alpha2;
v1=t.^2.*exp(-a*t).*cos(2*pi*f*t.^2).*(1/2+1/2*sign(t));
v2=alpha1+ beta1* (-beta1*t+tau1).^2.* exp(-a*(-beta1*t+tau1)).*cos(2*pi
    *f*(-beta1*t+tau1).^2).*(1/2+1/2*sign(-beta1*t+tau1));
v3=alpha3+ beta3*  (beta3*t+tau3).^2.* exp(-a*( beta3*t+tau3)).*cos(2*pi
    *f*( beta3*t+tau3).^2).*(1/2+1/2*sign( beta3*t+tau3));
rho21=v1*v2'/(v1*v1');
rho31=v1*v3'/(v1*v1');
nu32=v2*v3'/(v1*v1');
rho32=(nu32*rho21-rho31)/(1-rho21^2);
gamma21=-rho21;
gamma31= rho32*rho21-rho31;
gamma32=-rho32;
w1=1*v1 +0*v2 +0 *v3;
w2=gamma21*v1 + 1* v2 +0*v3;
w3=gamma31*v1 + gamma32*v2 + 1*v3;
figure(1);plot(t,v1,t,v2,t,v3);figure(2);plot(t,w1,'k',t,w2,'r',t,w3,'g'
    );
```

Appendix A.6. Some Definitions

- $\text{Rect}_T(t) = \begin{cases} 0 & \text{if } |t| > T/2 \\ 1/2 & \text{if } |t| = T/2 \\ 1 & \text{if } |t| < T/2. \end{cases}$
- $\text{Tri}_T(t) = \begin{cases} 1 - |t/T| & \text{for } |t| \le T \\ 0 & \text{otherwise} \end{cases}$

- $\text{sgn}(t) = \begin{cases} -1 & \text{if } t < 0 \\ 0 & \text{if } t = 0 \\ 1 & \text{if } t > 1. \end{cases}$
- $\text{III}_T(t) = \sum_{k=-\infty}^{+\infty} \delta(t - kT)$;
- $\delta(t) = \begin{cases} 1 & \text{if } t = 0 \\ 0 & \text{if } t \neq 0. \end{cases}$
- $u(t) = \begin{cases} 0 & \text{if } t < 0 \\ 1/2 & \text{if } t = 0 \\ 1 & \text{if } t > 0. \end{cases}$
- $\text{sinc}(t) = \frac{\sin(\pi t)}{(\pi t)}$ where $\text{sinc}(n) = 0 \; \forall n \in \mathbb{Z}^*$;
- $x(t) * y(t) = \int x(\tau) y(\tau - t) d\tau$;
- Scalar product of a signal of finite energy: $\langle x, y \rangle_t = \int_{t_1}^{t_2} x(t) y(t) \text{d}t$;
- Scalar product of a periodic signal of period T: $\langle x, y \rangle_t = \frac{1}{T} \int_{t_1}^{t_1+T} x(t) y(t) \text{d}t$.
- $HT[x(t)] = \frac{1}{\pi} \int_{-\infty}^{+\infty} \frac{x(\tau)}{(t-\tau)} d\tau$;
- $FT[x(t)] = \int_{-\infty}^{+\infty} x(t) \text{e}^{-2\pi j f t} dt$;
- Weighted Hermite polynomials: $(-1)^n \frac{\text{d}^n \text{e}^{-t^2}}{\text{d}t^n}$;
- orthogonal Haar decomposition: $\psi_{m,k}(t) = \psi(2^{m/2} t + k)$ with $\psi(t) = 1 \; \forall \; 0 \leq t \leq 1/2$, $\psi(t) = -1 \; \forall \; 1/2 \leq t < 1$ and $\psi(t) = 0$ otherwise;
- Rademacher orthogonal decomposition: $\psi_k(t) = \text{sgn}\left(\sin(2^k \pi t / T)\right)$.

Appendix A.7

See Table 1.

Table 1 First group (G1): finite energy signals with compact support. Second group (G2): even signals of finite energy. Third group (G3): causal signals of finite energy. Fourth group (G4): signals at finite average power (periodic). For all groups, solutions with singularities: 1–2, 8–9, 17–19

Group	Method	HT	d/dt	block-pulse
G1	$x_1(t) = Rect_T(t)$	$\tilde{x}_1(T/2) = \frac{1}{\pi} log \left\lvert \frac{t+\frac{T}{2}}{t-\frac{T}{2}} \right\rvert$	$\dot{x}_1(t) = \delta(t+\frac{T}{2}) - \delta(t+\frac{T}{2})$	$\hat{x}_1(t) = x_1(t-T)$
	$x_2(t) = Tri_T(t)$	$\tilde{x}_2(t) = -\tilde{x}_1(T) + \frac{t}{T\pi} log \left\lvert \frac{t^2}{t^2-T^2} \right\rvert$	$\dot{x}_2 = -sgn(t) Rect_{2T}(t)$	$\hat{x}_2(t) = x_2(t-2T)$
	$x_3(t) = x_1(t)x_{15}(t)$	$\tilde{x}_3 = cos(\frac{2\pi}{T}t) Rect_T(t)$	$\dot{x}_3(t) = \frac{2\pi}{T} cos(\frac{2\pi}{T}t) Rect_T(t)$	$\hat{x}_3(t) = x_3(t-T)$
G2	$x_4(t) = a/(a^2+t^2)$	$\tilde{x}_4(t) = t/(a^2+t^2)$	$\dot{x}_4(t) = -2at/(a^2+t^2)^2$	-
	$x_5(t) = sinc(\omega t)$	$\tilde{x}_5(t) = \frac{1-cos(\omega t)}{\omega t}$	$\dot{x}_5(t) = \omega \frac{\omega cos(\omega t) - sin(\omega t)}{(\omega t)^2}$	$\hat{x}_5(t) = x_5(t-T)$
	$x_6(t) = x_{14}(t)x_7(t)$	$\tilde{x}_6(t) = sin(\omega t)e^{-at^2}$	$\dot{x}_6(t) = \dot{x}_{15}(t)x_7(t) + x_{15}(t)\dot{x}_7(t)$	–
	$x_7(t) = e^{-at^2}$	–	$\dot{x}_7(t) = -2at\, x_7(t)$	–
G3	$x_8(t) = x_1(t-\frac{T}{2})$	$\tilde{x}_8(T/2) = \frac{1}{\pi} log \left\lvert \frac{t}{t-T} \right\rvert$	$\dot{x}_8(t) = \delta(t) - \delta(t+T)$	$\hat{x}_8(t) = x_1(t-\frac{T}{2})$
	$x_9(t) = x_2(t)x_8(t)$	$\tilde{x}_9(t) = \frac{T-t}{T\pi} log \left\lvert \frac{t}{t-T} \right\rvert + \frac{1}{\pi}$	$\dot{x}_9(t) = -Rect_T(t)$	$\hat{x}_9(t) = x_9(t-T)$
	$x_{10}(t) = e^{-at}u(t)$	–	–	$\hat{x}_{10}(t) = x_{10}(-t)$
	$x_{11}(t) = te^{-t^2}u(t)$	–	–	$\hat{x}_{11}(t) = x_{11}(-t)$
	$x_{12}(t) = tx_{10}(t)$	–	–	$\hat{x}_{12}(t) = x_{12}(-t)$
	$x_{13}(t) = x_{14}(t)x_{10}(t)$	–	–	$\hat{x}_{13}(t) = x_{13}(-t)$
G4	$x_{14}(t) = cos(\frac{2\pi}{T}t)$	$\tilde{x}_{14}(t) = sin(\omega t)$	$\dot{x}_{14}(t) = -\omega \tilde{x}_{14}(t)$	–
	$x_{15}(t) = sin(\frac{2\pi}{T}t)$	$\tilde{x}_{15}(t) = cos(\frac{2\pi}{T}t)$	$\dot{x}_{15}(t) = \frac{2\pi}{T}\tilde{x}_{15}(t)$	–
	$x_{16}(t) = \lvert x_{14}(t) \rvert$	–	$\tilde{x}_{16}(t) = -\dot{x}_{14}(t)\tilde{x}_1(T/2) * \text{III}_{T/2}(t)$	–
	$x_{17}(t) = x_1(t) * \text{III}_{2T}(t)$	$\tilde{x}_{17} = \tilde{x}_1(T/2) * \text{III}_{2T}(t)$	$\dot{x}_{17}(t) = \dot{x}_1(t) * \text{III}_{2T}(t)$	–
	$x_{18}(t) = x_2(t) * \text{III}_{2T}(t)$	$\tilde{x}_{18} = \tilde{x}_2 * \text{III}_{2T}(t)$	$\dot{x}_{18}(t) = \dot{x}_2(t) * \text{III}_{2T}(t)$	–
	$x_{19}(t) = x_9(t) * \text{III}_T(t)$	$\tilde{x}_{19} = \tilde{x}_9 * \text{III}_T(t)$	$\dot{x}_{19}(t) = \dot{x}_9(t) * \text{III}_T(t)$	–

References

1. O.M. Boaghe, S.A. Billings, Subharmonic oscillation modeling and miso Volterra series. IEEE Trans. Circuits Syst. **50**, 877–884 (2003)
2. T.T. Cai, L. Wang, Orthogonal matching pursuit for sparse signal recovery with noise. IEEE Trans. Inf. Theory **57**, 4680–4688 (2011)
3. S. Chen, S.A. Billings, W. Luo, Orthogonal least squares methods and their application to non-linear system identification. Int. J. Control **50**, 1873–1896 (1989)
4. M. Ciobotaru, R. Teodorescu, F. Blaabjerg, A new single-phase pll structure based on second order generalized integrator, in *37th IEEE Power Electronics Specialists Conference* (2006), pp. 1–6
5. M.S. Corrington, Solution of differential and integral equations with Walsh functions. IEEE Trans. Circuit Theory **5**, 470–476 (1973)
6. K.B. Datta, B.M. Mohan, *Orthogonal Functions in Systems and Control*, vol. 9 (World Scientific, Singapore, 1995)
7. I. Galkin, M. Vorobyov, Optimizing of sampling in a low-cost single-phase instantaneous ac-grid synchronization unit with discrete calculation of derivative function, in *41st Annual Conference of the IEEE Industrial Electronics Society* (2015), pp. 4538–4543
8. S. Gautam, W. Hassan, A. Bhatta, D. D.-C. Lu, W. Xiao, A comprehensive study of orthogonal signal generation schemes for single phase systems, in *1st IEEE International Conference on Power Electronics and Energy* (2021), pp. 1774–1782
9. J.P. Gram, Om rackkendvilklinger bestemte ved hjaelp af de minfste kvadraters methode, Copenhagen, 1879, translated in German as: Über die entwicklung reeller funktionen in reihen mittels der methode der kleinsten quadrate. J. reihe angew. Math. **94**, 41–73 (1883)
10. S.L. Hahn, *Hilbert Transforms in Signal Processing*, vol. 2 (Artech House, Boston, 1996)
11. Y. Han, M. Luo, X. Zhao, J.M. Guerrero, L. Xu, Comparative performance evaluation of orthogonal-signal-generators-based single-phase pll algorithms: a survey. IEEE Trans. Power Electron. **31**, 3932–3944 (2016)
12. H.F. Harmuth, *Transmission of Information by Orthogonal Functions*, 1st edn. (Springer, New York, 1972)
13. R.-Y. Kim, S.-Y. Choi, I.-Y. Suh, Instantaneous control of average power for grid tie inverter using single phase dq rotating frame with all pass filter, in *30th Annual Conference of IEEE Industrial Electronics Society* (2004), pp. 274–279
14. F.W. King, *Hilbert Transforms*, vol. 2 (Cambridge University Press, Cambridge, 2009)
15. L.M. Kunzler, L.A. Lops, Wide frequency band single-phase amplitude and phase angle detection based on integral and derivative actions. Electronics **9**, 1578–1600 (2020)
16. P. Lamo, A. Pigazo, F.J. Azcondo, Evaluation of quadrature signal generation methods with reduced computational resource for grid synchronization of single-phase power converters through phase-locked loops. Electronics **9**, 2026–2048 (2020)
17. B. Le Floch, M. Alard, C. Berrou, Coded orthogonal frequency division multiplex. Proc. IEEE **83**, 982–996 (1995)
18. A. Luo, Y. Che, Z. Shuai, C. Tu, An improved reactive current detection and power control method for single-phase photovoltaic grid-connected dg system. IEEE Trans. Energy Convers. **28**, 823–831 (2013)
19. S. Mallat, *A Wavelet Tour of Signal Processing. The Sparse Way*, 3er edn. (Elsevier, Amsterdam, 2008)
20. A.D. Poularikas, *Transforms and Applications Handbook*, 3er edn. (CRC Press, Taylor and Francis Group, London, 2010)
21. L. Rebollo-Neira, D. Lowe, Optimized orthogonal matching pursuit approach. IEEE Signal Process. Lett. **9**, 137–140 (2002)
22. M. Renfors, X. Mestre, E. Kofidis, F. Bader, *Orthogonal Waveforms and Filter Banks for Future Communication Systems* (Academic Press, London, 2017)
23. M. Saitou ,T. Shimizu, Generalized theory of instantaneous active and reactive powers in single-phase circuits based on Hilbert transform, in *33rd Annual IEEE Power Electronics Specialists Conference* (2002), pp. 1419–1424
24. C. H. Savit, Method for generating orthogonal sweep signals. US Patent 4 686 654 (1987)
25. F. Sbeity, S. Ménigot, J. Charara, J.-M. Girault, A general framework for modeling sub- and ultraharmonics of ultrasound contrast agent signals with miso Volterra series. Comput. Math. Methods Med. (2013). https://doi.org/10.1155/2013/934538

26. E. Schmidt, Zur theorie der linearen und nicht linearen integralgleichungen zweite abhandlung. Math. Ann. **64**(2), 161–174 (1907)
27. Y.V. Stasev, N. Naumenko, A. Kuznetsov, The derivative orthogonal signals systems. Int. J. Eng. Pract. Res. **1**(1), 15–20 (2012)
28. F.M. Stein, Orthogonal functions whose kth derivatives are also orthogonal. SIAM Rev. **1**(2), 167–170 (1959)
29. L.M. Surhone, M.T. Timpledon, S.F. Marseken, *Orthogonality: Orthogonalization, Gram–Schmidt Process, Orthogonal Complement, Orthonormality, Split-quaternion* (Betascript Publishing, Beau-Bassin, 2010)
30. Y. Triki, A. Belouche, H. Seddiki, D.O. Abdelslam, Evaluation of quadrature signal generation methods with reduced computational resource for grid synchronization of single-phase power converters through phase-locked loops. Eur. J. Electr. Eng. **23**, 113–122 (2021)
31. L. Xiong, F. Zhuo, X. Wang, M. Zhi, A fast orthogonal signal-generation algorithm characterized by noise immunity and high accuracy for single-phase grid. IEEE Trans. Power Electron. **31**, 1847–1851 (2016)
32. M. Yaghoobi, D. Wu, M.E. Davies, Fast non-negative orthogonal matching pursuit. IEEE Signal Process. Lett. **22**, 1229–1233 (2015)
33. R. Zhang, M. Cardinal, P. Szczesny, M. Dame, A grid simulator with control of single-phase power converters in dq rotating frame, in *33rd IEEE Power Electronics Specialists Conference. Proceedings*, vol. 3 (2002), pp. 1431–1436